Cranial morphology in *Mollisquama* sp. (Squaliformes; Dalatiidae) and patterns of cranial evolution in dalatiid sharks

John S. S. Denton,[1] (iD) John G. Maisey,[1] Mark Grace,[2] Alan Pradel,[3] Michael H. Doosey,[4] Henry L. Bart Jr[4] and Gavin J. P. Naylor[5]

[1]*Department of Vertebrate Paleontology, American Museum of Natural History, New York, NY, USA*
[2]*NOAA/Southeast Fisheries Science Center/NMFS/Mississippi Laboratories, Pascagoula, MS, USA*
[3]*UMR 7207 CR2P - Muséum National d'Histoire Naturelle, CNRS, Sorbonne Université Paris, Paris, France*
[4]*Tulane University Biodiversity Research Institute, Belle Chasse, LA, USA*
[5]*Florida Program for Shark Research, Florida Museum of Natural History, University of Florida, Gainesville, FL, USA*

Abstract

Dalatiid sharks are members of a family of predominantly small, midwater meso- and bathypelagic chondrichthyans. The family is notable for both its number of monotypic genera and high morphological disparity. Three of the seven dalatiid genera are known only from holotype specimens (*Mollisquama parini*) or from only a handful of specimens (*Euprotomicroides zantedeschia*, *Heteroscymnoides marleyi*), with the only detailed anatomical work consistent across all taxa being studies of dentition. Here, we present detailed anatomical description of the second-ever specimen of *Mollisquama* (*Mollisquama* sp.) covering chondrocranial, jaw, dental, and muscular anatomy, derived from a phase-contrast synchrotron microtomographic scan. *Mollisquama* sp. is unique among dalatiids in possessing a deep carinal process, extending ventrally from the bar between the subethmoid region and basal angle in squaloid sharks, containing a large fenestra infiltrated by the suborbitalis muscle. *Mollisquama* sp. also exhibits additional possibly diagnostic features, including a planar configuration of the labial cartilages and the absence of labial folds; a pad-like orbital process on the palatoquadrate; and the origination of the suborbitalis muscle solely on the carina, rather than the intraorbital wall. Character optimization of anatomical data onto a phylogeny of dalatiid sharks suggests *Mollisquama* sp. to be among the most specialized in the family, expanding the existing dalatiid morphospace. However, the functional significance of such transformations remains unclear. Synchrotron-derived data, which do not require chemical pretreatment of specimens, may elucidate soft-tissue functional correlates in future studies of undersampled taxa, such as dalatiids.

Key words: chondrocranium; ectoparasitism; midwater; synchrotron; teeth

Introduction

Dalatiid sharks (Squaliformes; Dalatiidae) are a family of midwater sharks comprising nine currently described species in seven genera. Dalatiid sharks are known for their predominantly small size, tooth morphology (dignathic heterodonty), and bioluminescent organs ranging from densely packed ventral countershading photophores (Claes & Mallefet, 2009) to complex abdominal (*Euprotomicroides* zantedeschia; Munk & Jørgensen, 1988) and pectoral (*Mollisquama*; Grace et al. 2015; Dolganov, 1984) secretory pouches. Previous morphological phylogenetic work incorporating dalatiid taxa (Shirai, 1992, 1996; de Carvalho, 1996) recovered distinct 'euprotomicrinine' (*Euprotomicrus*, *Squaliolus*) and 'dalatiine' (*Dalatias*, *Isistius*) clades (*sensu* Shirai, 1992, 1996) also recovered by cladistic analysis of dental characters (Adnet & Cappetta, 2001). However, beyond the character selection and sampling used by these large-scale analyses, little is known about dalatiid anatomy and functional morphology.

Of the dalatiid taxa, the Cookiecutter Shark, *Isistius brasiliensis*, has received the most attention, given its extreme dignathic heterodonty and conspicuous ectoparasitic feeding strategy (Jones, 1971; Papastamatiou et al. 2010; Dwyer & Visser, 2011; Hoyos-Padilla et al. 2013; Best &

Photopoulou, 2016), and the role of its bite marking in the forensic analysis of human remains (Makino et al. 2004; Hayashi et al. 2015; Ribéreau-Gayon et al. 2017). In *Isistius,* feeding is accomplished via scooping of the jaw and twisting of the body to extract a tissue plug from prey, and ingestion of the plug via strong negative pressure generation in the buccal cavity (Shirai & Nakaya, 1992). *Isistius* exhibits numerous anatomical specializations for this feeding mode, including highly reduced lanceolate upper dentition, a reduced nasal capsule, a subdivided palatoquadrate, enlarged labial folds, enlarged basihyal, direct contact between the rectus cervicus and hypaxial muscles, and rigid attachment of the ligamentum mandibulo-hyoideum to the ceratohyal and mandibular below the ceratohyal-hyomandibular articulation point (Shirai, 1992; Shirai & Nakaya, 1992). No functional anatomy in any other dalatiid is as well known.

A major reason for the lack of morphological data in dalatiids is likely insufficient sampling among the rarer taxa: one of the seven genera is known from a single specimen (*Mollisquama parini*; Dolganov, 1984), another from two specimens (*Euprotomicroides zantedeschia*; Munk & Jørgensen, 1988), and another from a handful of specimens (*Heteroscymnoides marleyi*; Stehmann et al. 1999). Recently, a second *Mollisquama* specimen was taken during a cetacean survey in the northern Gulf of Mexico (Grace et al. 2015), and was provisionally assigned to the genus *Mollisquama* based on the presence of the pectoral pocket gland, as well as diagnostic dalatiid characters (Grace et al. 2015). However, additional characters, including the presence of ventral photophores, dermal denticle spatial configuration, tooth morphology, and vertebral counts, precluded its assignment to *M. parini*. The small number of *Mollisquama* specimens provides a limiting case for anatomical study, as destructive, dissection-based work is prohibitive and, despite the revolution in soft-tissue microCT-based imaging methods (Metscher, 2009; Gignac et al. 2016), the potential separate species status of the two *Mollisquama* makes the chemical treatment required for enhancing microCT tissue contrast problematic. Here, to expand our understanding of dalatiid cranial morphology and function, we present descriptive anatomy on the chondrocranium, oral jaws, dentition, hyoid arch, and primary cranial musculature of the second *Mollisquama* specimen, based on propagation phase-contrast X-ray synchrotron microtomography, a technique which can recover soft tissue detail without chemical treatment.

Materials and methods

Digital imaging and segmentation

The *Mollisquama* sp. specimen (TU 203676) was scanned at the European Synchrotron and Radiation Facility, Grenoble, France (ESRF), on beamline ID019 using propagation phase-contrast X-ray synchrotron microtomography. Scanning achieved a 6.24-μm voxel size, with an average detected energy of 102.9 keV, using 5.6 mm Al and 4 mm Cu filters, a PCO edge 5.5 sensor, a W150 insertion device, and a LuAG:Ce 500-μm scintillator. The propagation distance was 7 cm and the ID gap was 51 mm. Scan geometry was 360°, half acquisition, in a vertical series of 23 sections, with an exposure time of 0.1 s. Images were reconstructed using the phase retrieval algorithm of Paganin et al. (2002). File size (> 200 Gb) made processing of the full stack impossible in any file format. A half-stack was opened in Fiji, sampling every fourth image, and the image sequence identifying the prescapular region was identified visually, after which the full, unskipped stack was extracted. Segmentation of this data was conducted in VGSTUDIOMAX v3.0 (Volume Graphics, 2016) at the Microscopy and Imaging Facility at the American Museum of Natural History.

Anatomical abbreviations

aa, anterior ampulla; am, adductor mandibulae; ams, adductor mandibulae superficialis; anf, anterior narial flap; ao pr, antorbital process; art pr, articular process (palatoquadrate); art cot, articular cotylus (Meckel's cartilage); asc, anterior semicircular canal; ba, basal angle of basicranium; bh, basihyal; bh art, basihyal-ceratohyal articulation; bpr, basipterygoid process; car, suborbital carina; car proc, process of suborbital carina; ch, ceratohyal; chd, constrictor hyoideus dorsalis; ch pr, ventral ceratohyal process; cr, chondrocranium; dend, endolymphatic duct; dgr, dental groove; emb, anterior embayment between palatoquadrates; end f, endolymphatic foramina; end fs, endolymphatic fossa; ea, external ampulla; esc, external semicircular canal; fica, foramen for internal carotid arteries; fl, floor of cranial cavity; fm, foramen magnum; hm, hyomandibula; hm art, hyomandibular articulation with cranium; hm VII, foramen for hyomandibular branch of facial nerve; lat com, lateral commissure; llab, lower labial cartilage; mb, main bar (palatoquadrate); Mc, Meckel's cartilage; mf, muscular furrow of hyomandibula; mk, mandibular knob; mnf, mesonarial flap; mpr, muscular process (palatoquadrate); n, notch between supraorbital and sphenotic ridge; nc, nasal cartilage; o art, orbital articulation; oca, occipital arch; oc cot, occipital cotylus; oc hem, occipital hemicentrum; olf c, olfactory capsule; olf tr, olfactory tract; onf, orbitonasal foramen; opr, orbital process (palatoquadrate); or, orbit; ora, foramen for orbital artery; pa, posterior ampulla; pac, preampullary canal; par, parachordal region of basicranium; per fen, perilymphatic fenestrae; pf, pituitary foramen; pin, notch for pineal organ; pnf, internal lobe of posterior narial flap; pnw, postnasal wall; popr, postorbital process; postot pr, postotic process; pq, palatoquadrate; pqcot, palatoquadrate cotylus; pr can, profundal canal; pr font, precerebral fontanelle; pr fs, precerebral fossa; psc, posterior semicircular canal; qcon, palatoquadrate condyle; rc, rostral cartilage; r fen, rostral fenestrae; sac, saccular chamber; so, suborbitalis; sof, spino-occipital foramina; soph, superficial ophthalmic foramina in supraorbital shelf; sphr, sphenotic ridge; sub fen, suborbital fenestra; sup r, supraorbital ridge; sup s, supraorbital shelf; sym, symphysis; tfr, trigemino-facialis recess; ualab, upper anterior labial cartilage; uplab, upper posterior labial cartilage; ur, utricular recess; II, optic foramen; III, oculomotor foramen; IV, trochlear foramen; VIII, octaval (statoacoustic) nerve; IX, glossopharyngeal canal or foramen; X, vagus foramen.

Dental abbreviations

apr, apron; cav, pulp cavity; cdh, canal of distal heel; cpc, canal of principal cusp; dce, distal cutting edge; dh, distal heel; drc, distal

root canal; labh, labial hollow; laxf, lower axial foramen (labial surface); mce, mesial cutting edge; mrc, mesial root canal; ovs, tooth overlapping surface (lingual surface); pc, principal cusp; r, root; uaxf, upper axial foramen (lingual surface).

Description

Chondrocranium

The ethmoidal region is much wider than long, with only a vestigial anterior extension of rostral median cartilage located entirely between olfactory capsules, and does not protrude anterior to them. Bulbous nasal capsules form the anterior extremity of chondrocranium and approach each other at the midline. The olfactory openings face anteriorly rather than anteroventrally or ventrally. The nasal capsules appear crumpled in the specimen (Fig. 1).

The rostral cartilage forms a narrow bar that extends posteriorly as a median keel that, as in many other 'squaloid' sharks, meets the basicranium below the orbit (Fig. 1C). The

bar is flanked by trapezoidal rostral fenestrae (paired openings that do not transmit nerves or blood vessels; Holmgren, 1941) that extend behind the olfactory capsules as far as the inner wall of the olfactory canals and traverse more than half the width of the olfactory capsules.

The anterior boundary of the intracranial space (defined by membranous dura surrounding the brain; see Supporting Information Fig. S1) is level with the posterior border of the rostral fenestrae; the space occupied by the brain does not extend above the rostral fenestrae. The precerebral fontanelle (anterior opening of the intracranial cavity = 'prefrontal fontanelle' of Shirai, 1992) is wide and subrectangular, with a dorsal notch for the pineal organ at its midline (Fig. 1A,E). The precerebral fossa (space anterior to the dura) is short and wide, and does not extend in front of the nasal capsules. The nasal cartilage (Fig. 2) possesses anteriorly directed, acuminate nasal flaps.

The ventral part of the ethmoidal region exhibits a deep suborbital carina, extending from between nasal capsules
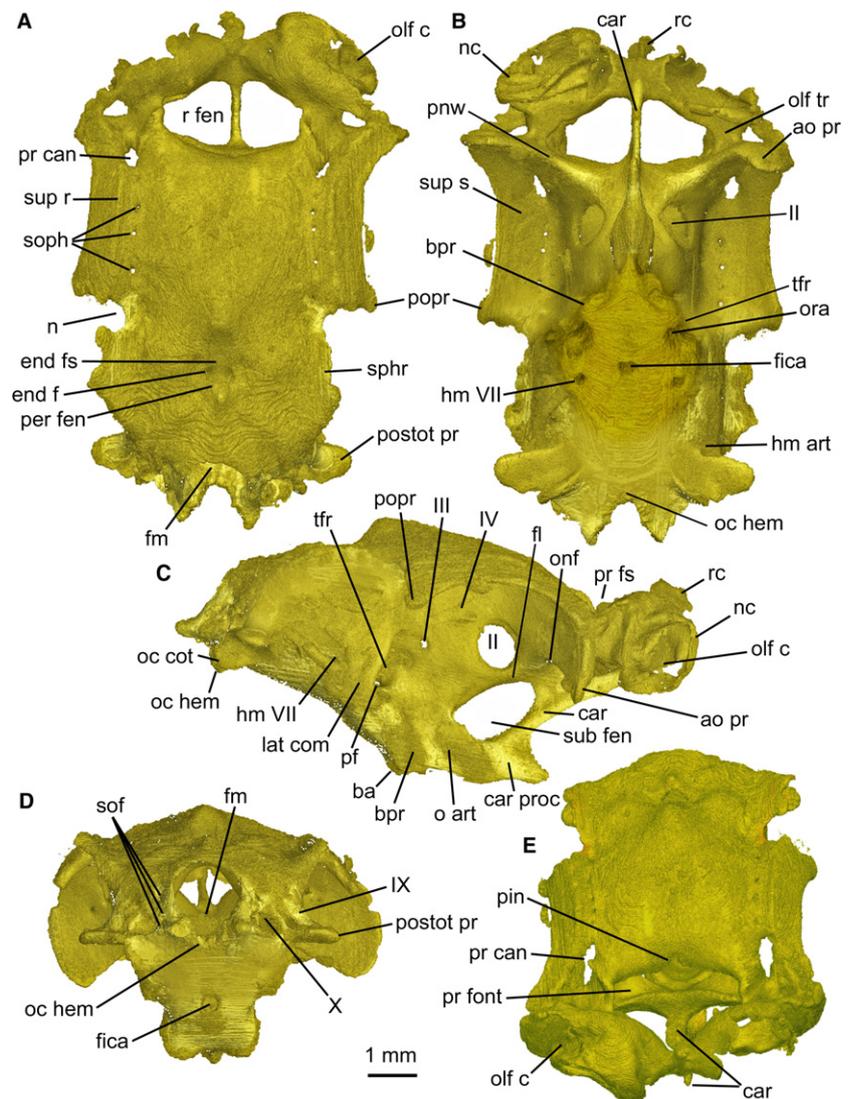

Fig. 1 *Mollisquama* sp., TU 203676, chondrocranium in (A) dorsal, (B) ventral, (C) lateral, (D) posterior, and (E) anterior views. Only one olfactory capsule was segmented. Anterior to top in (A) and (B), to right in (C).
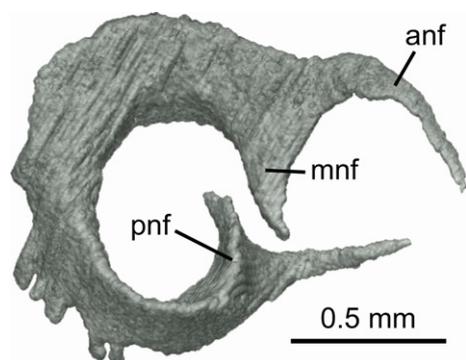
Fig. 2 *Mollisquama* sp., TU 203676, nasal cartilage from right side, viewed anterolaterally.

and meeting the basicranium just anterior to the orbital articulation. The suborbital carina contributes to the origin of suborbitalis musculature (see below) and is the most heavily calcified part of the ethmoid region. The suborbital carina bears a stout, anteriorly directed process posteroventrally and is pierced by a large oval fenestra between the carinal process and optic nerve foramen in the orbit; fenestra roof forms the floor of cranial cavity. The suborbital carina is associated with extreme acuity of the basal angle (a fold between chordal and prechordal parts of basicranium, formed secondarily during ontogeny by upward rotation of embryonic trabecular cartilages with respect to polar and parachordal cartilages; El-Toubi, 1949; Holmgren, 1940; Jollie, 1971). *Mollisquama* sp. lacks an ectethmoid chamber; instead, the postnasal (orbitonasal) wall forms a paddle-shaped antorbital process that forms the widest part of chondrocranium and is continuous with the supraorbital shelf (Fig. 1B). Only the ventral border of the antorbital process is calcified in the specimen. The postnasal wall contains a small orbitonasal foramen.

The lateral margin of the supraorbital shelf is slightly curved and forms a wide roof to the orbit. Each shelf is penetrated by a series of three or four superficial ophthalmic foramina, which are located within a shallow anteroposterior sulcus on the upper surface of the shelf. The shelf is thickened lateral to the ophthalmic foramina, forming a low, anteroposteriorly directed supraorbital ridge. The preorbital canal penetrates the roof of the orbit anterior to the supraorbital ridge. Anterior to the ophthalmic foramina there are two divergent sulci; the more medial one (possibly for the ophthalmic branch) passes obliquely across the roof of the olfactory canal and the other one (possibly for the ethmoidal branch after it separated from the ophthalmic branch) passes anterolaterally towards another large foramen positioned lateral to the olfactory canal. The posterior end of the supraorbital shelf projects sharply from the cranial wall. It bears a rounded posterolateral apex (Fig. 1A,B), which corresponds topographically to the 'primary' component of the postorbital process (Holmgren, 1940, 1941; the postorbital process in chondrichthyans may include

cartilage derived from the embryonic lateral commissure in addition to the 'primary' process).

The floor of the cranium below the optic foramen is smooth and convex from side to side. Foramina within the orbit are arranged much as in other elasmobranchs, with a centrally located optic foramen, behind which are small trochlear and oculomotor foramina, plus a shallow pit in the expected position of the optic pedicel. However, the pedicel could not be found and may be absent. Configuration of the rectus muscles was not determined, but the posterior part of the orbit is occupied by a deep trigemino-facialis recess, containing foramina for major branches of facial and trigeminal nerves and the external rectus muscle.

The lateral wall of the trigemino-facialis recess is well developed and the lateral commissure is extensively chondrified. The dorsal end of the commissure merges with the braincase side wall below the level of supraorbital shelf and does not meet the postorbital process located farther dorsally (see Supporting Information Fig. S2). The hyomandibular branch of the facial nerve exits the braincase on the lower part of the lateral surface (Fig. 1B,C) through the foramen located some distance posterior to the commissure. The orbital articulation is well developed (Fig. 1C) and located ventral to the trigemino-facialis recess, and its articular surface includes paired basitrabecular processes (*sensu* Shirai, 1992) that are bulbous and rounded. The dorsal part of the basitrabecular process is separated from the ventral end of the lateral commissure by a narrow sulcus, which contains a foramen for the pituitary vein. Medial to the basitrabecular process there is a smooth, concave groove that houses the orbital process of the palatoquadrate. Posterior to the orbital articulation, the basicranium becomes progressively wider and is gently convex from side to side. There is a single opening at the ventral midline for paired internal carotid arteries and lateral to these are paired foramina for orbital arteries, plus another pair farther posteriorly, probably for the hyoid/palatine ramus of the facial nerve.

The otic region is deepest at the boundary between the orbital and otic regions, and tapers posteriorly. The lateral wall of the otic capsule is flared laterally, forming a prominent and well calcified sphenopterotic ridge (*sensu* Shirai, 1992) that forms the surface of origin of the constrictor dorsalis muscle. The sphenopterotic and supraorbital shelves are separated by a deep, rounded notch. The posterior end of the supraorbital shelf is downturned ventral to the sphenopterotic ridge. The two shelves are not confluent, and the constrictor dorsalis muscle does not extend into this notch (see below). The sphenopterotic ridge curves downward and diminishes in height posteriorly, terminating a short distance dorsal to the articular facet for the hyomandibula.

The skeletal labyrinth of the otic region (Fig. 3) measures 3 mm anteroposteriorly between anterior and

posterior ampullae. The posterior semicircular canal forms an almost complete circuit (meeting the saccular chamber posteromedially), and the perilymphatic fenestra opens dorsally (Figs 1 and 3). Based on the orientation of the external (horizontal) canal, the labyrinth is slightly upturned anteriorly relative to the vertebral axis. The floor of the glossopharyngeal canal extends laterally, forming a prominent post-otic process (*sensu* Holmgren, 1941), as in many other modern elasmobranchs. The hyomandibular facet at the posterolateral margin of the otic capsule is ventral to the post-otic process (Fig. 1C). The vagus nerve opening is located medial to the posterior ampulla and lateral to the occipital hemicentrum. The endolymphatic fossa is small and slightly wider than long (Fig. 1A). Details of openings within the fossa were difficult to determine, but there is apparently a small pair of endolymphatic foramina anterior to the larger paired perilymphatic fenestrae (see Supporting Information Fig. S3).

The occipital region is extremely short, and an occipital hemicentrum is present within the thickness of the basicranial cartilage (Fig. 1D). The basicranial cartilage surface both dorsal and ventral to the occipital half centrum is calcified, as are the internal and external side walls of the occipital arch. At least three paired spino-occipital nerve foramina pass through the calcified parts of occipital arch. On the internal surface of the occipital arch, openings are arrayed anteroposteriorly on each side, as in most elasmobranchs, but their posterior exits are stacked one above the other, with the lowest (posteriormost) exit just level with

the top of the half centrum, and those farther anteriorly exit progressively higher in the side wall of the occipital arch. Paired occipital condyles are below the occipital arch and medial to the vagus canal.

The only mineralized parts of the chondrocranium are the chordal part of the basicranium from the occipital region to just anterior to the internal carotid foramina, much of the suborbital carina, the ventral part of the post-nasal wall, the ventral surface of the primary postorbital process, the sphenotic ridge, the dorsal surface of the post-otic process, and the side walls of the occipital arch (Fig. 4). Additionally, the occipital hemicentrum is calcified along with the vertebral centra. The chordal basicranium (par), formed in the embryonic parachordal cartilages, is the most
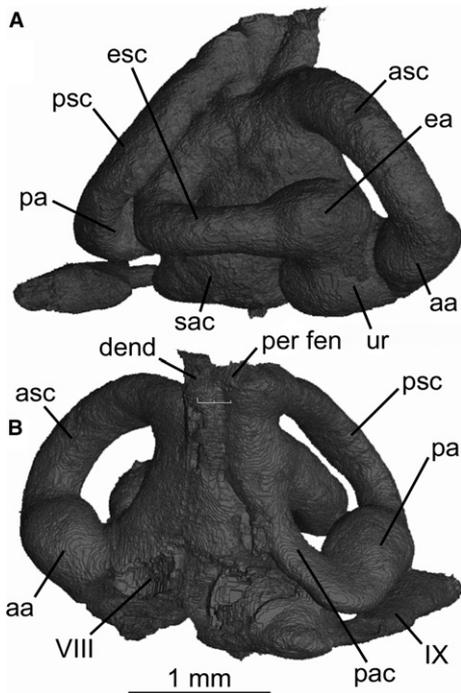

Fig. 3 *Mollisquama* sp., TU 203676, right skeletal labyrinth in (A) lateral and (B) medial view.
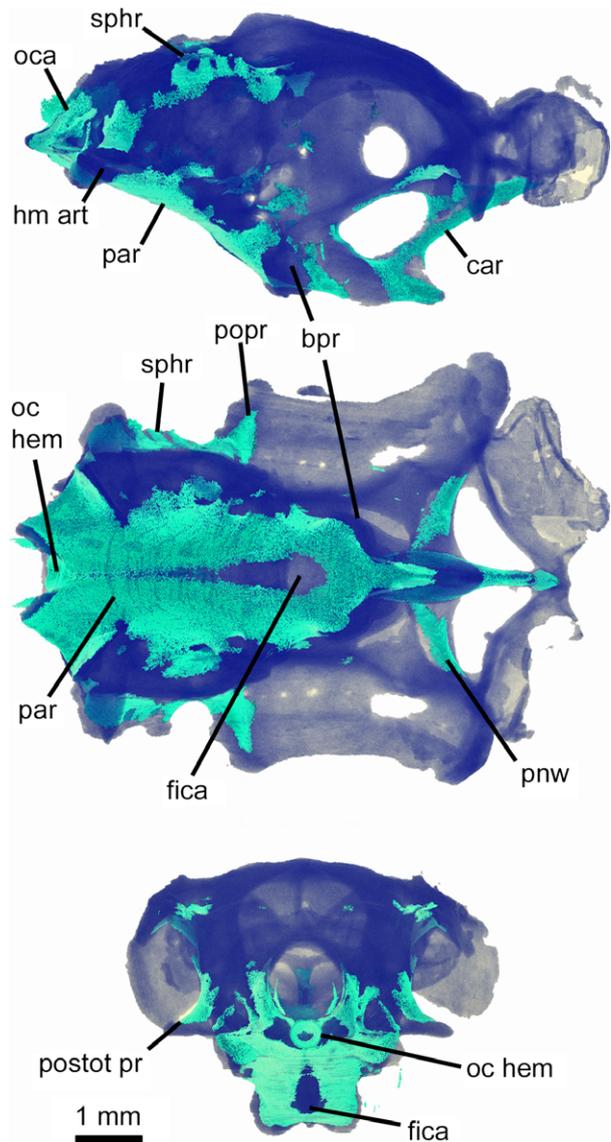

Fig. 4 *Mollisquama* sp., TU 203676, chondrocranium showing extent of mineralization; unmineralized cartilage is shown in dark blue, mineralized areas in turquoise.

extensively calcified region of chondrocranium. On the undersurface of the cartilage (i.e. external basicranium), perichondral calcification extends from base of suborbital keel to occipital region, with a large, teardrop-shaped uncalcified area mid-ventrally (around the hypophyseal region). However, on the internal (intracranial) surface of the cartilage, paired subrectangular calcified regions extend from the base of occipital arch only as far as mid-way between the occiput and hypophysis; these calcified areas are united only posteriorly and the space between them widens anteriorly.

Jaws

As in other dalatiids, *Mollisquama* sp. jaws are abbreviated and do not extend to the ethmoid region, and the entire mandibular arch is tilted downward (Fig. 5). The palato-quadrates are entirely separated by a narrow symphysis. The deep symphysis between the Meckel's cartilages has two distinct parts; in its upper half, the cartilages almost meet at the midline, but in the lower part there is a wider space between them. The palatoquadrate is not subdivided into separate palatine and quadrate components as in *Isistius* (Shirai, 1992: char. 57). Following the terminology of the palatoquadrate in *Squalus* by Haller (1926), the cartilage in *Mollisquama* sp. comprises four main regions; a tooth-bearing arch piece (main bar), an orbital process (articulating with the braincase), a muscular process (=otic flange of Shirai, 1992), and an articular process (Fig. 6A–E). The arch piece includes the tooth-bearing ventral lingual margin of the palatoquadrate. The tooth-bearing dental groove contains developing (non-functional) teeth lin-gually, and functional teeth further labially. There is no sharp demarcation between functional and developing upper teeth. There is a deep embayment in the upper surface of the arch piece anterior to the base of the orbital process that encloses part of the suborbital carina. A similar embayment is present in *Etmopterus* (Shirai, 1992: Pl. 24A) but is absent in *Dalatias*. The articular process extends ventrocaudally from the arch piece and bears an articular condyle for lower jaw. The muscular process arises from the dorsolateral part of arch piece and extends laterally between the mandibular joint and the apex of the muscular process. The palatoquadrate posterior margin is gently convex. There is a quadrate concavity for the mandibular knob on the mesial surface of the palatoquadrate, slightly anterior to the articular process (Fig. 6B).

The orbital process is low and wide, and extends dorsally from the mediodorsal margin of the arch piece into the ventral part of orbit, where it articulates with the basipterygoid process of the chondrocranium. The oral margin is angled between the anterior (tooth-bearing) and posterior regions, placing the mandibular joint posteroventral to the occlusal surface.

The labial and lingual surface of Meckel's cartilage is sharply demarcated by a narrow oral margin, with functional teeth arrayed along the upper edge of the labial surface, while the rows of developing teeth cover much of its lingual surface. Features associated with the mandibular joint include an articular cotylus, which is located on a short outer process (Haller, 1926), plus a mandibular knob (*sensu* Hotton, 1952) situated farther medially. There is a low process on the dorsolateral margin of Meckel's cartilage, anterior to the mandibular joint, and lateral to the posterior part of the dental groove and the oral margin of the palatoquadrate. The anterior margin of Meckel's cartilage is deep, but it only meets its antimere in the dorsal half of the symphysial region; farther ventrally, the cartilages are separated by a parallel-sided gap (Fig. 6H,I).

The three pairs of labial cartilages (two upper, one lower) correspond topographically to those in *Squalus acanthias* (Haller, 1926; Wolfram, 1984). The lower and upper posterior cartilages lie along the anterior border of the suborbitalis muscle and are bound together in the angle of the mouth at a highly obtuse (almost straight) angle (Fig. 7). The upper posterior labial element is narrower than the anterior one, the reverse arrangement to most dalatiids. It is a needle-like element with a pointed anterior and club-like posterior end. The upper anterior labial has a flattened and slightly expanded dorsal end that extends behind the upper posterior. The lower labial element is by far the
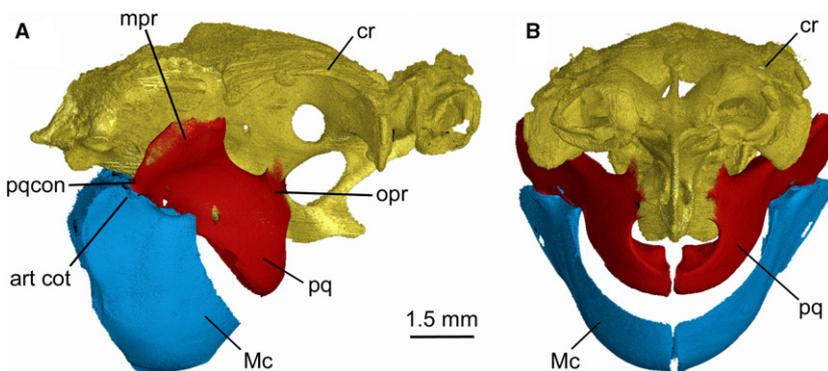

Fig. 5 *Mollisquama* sp., TU 203676, chondrocranium and jaws in (A) right lateral and (B) anterior view. Chondrocranium appears gold, palatoquadrates red, Meckel's cartilages blue.
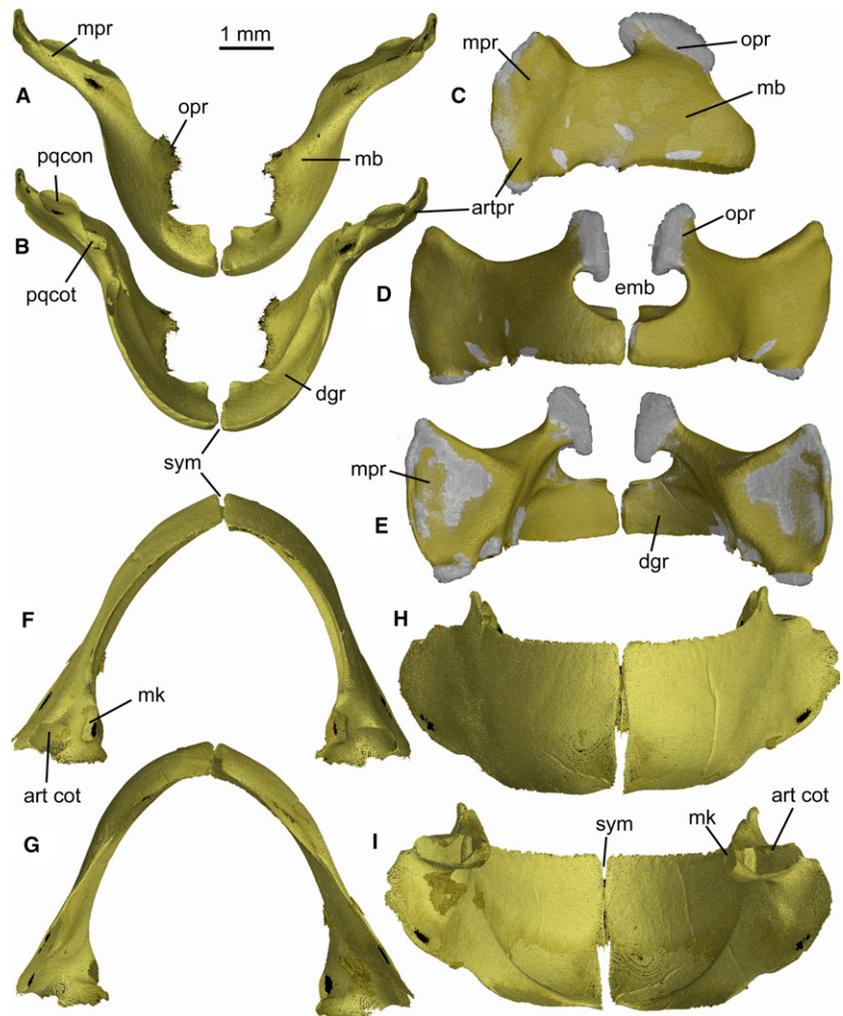
Fig. 6 *Mollisquama* sp., TU 203676, jaw cartilages; (A–E) palatoquadrates, (F–I) Meckel's cartilages. (A,F) dorsal views; (B,G) ventral views; (C) lateral view of right palatoquadrate; (D,H) anterior views; (E,I) posterior views. Mineralized areas appear gold, unmineralized areas gray.
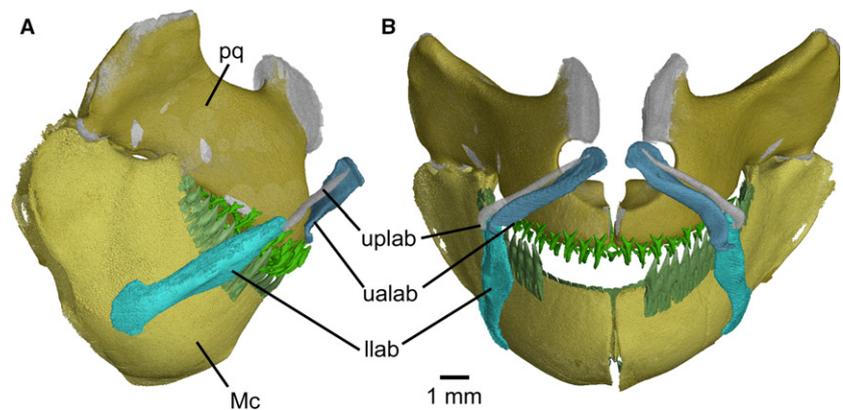

Fig. 7 *Mollisquama* sp., TU 203676, jaws and labial cartilages in (A) right lateral and (B) anterior views. Gap in dentition on Meckel's cartilages due to missing teeth.

largest of the three elements, with a rounded, bladelike ventral end.

Teeth and dentition

The *Mollisquama* dentition exhibits strong dignathic heterodonty and weak gradient monognathic heterodonty, with a low number of tooth families. The upper and lower teeth overlap anteriorly, but farther posteriorly a slight underbite is present. The upper and lower dentitions both include a single symphyseal tooth family. Three to four teeth are present in each family of upper teeth (Fig. 8). Four teeth are present in each lower tooth family: a single functional (upright) tooth, two completely-formed but still-

inverted replacement teeth, plus the calcified cutting edges of a developing tooth crown (also inverted), located deep within the dental lamina (Fig. 9). Mineralization of developing teeth in *Mollisquama* sp. evidently began with enameloid deposition at the apex and along cutting edges of principal cusp and heel.

The upper teeth do not overlap or imbricate, but teeth in adjacent families occupy alternating positions (Fig. 8A,B). Each upper tooth has a narrow, pointed single median cusp and no lateral cusps (Fig. 8C–F). The upper tooth crowns are conical, with no cutting edge or apron, and the root has distinct mesial and distal lobes that become progressively less well developed in more posterior teeth; between the mesial and distal lobes, a single median external foramen is
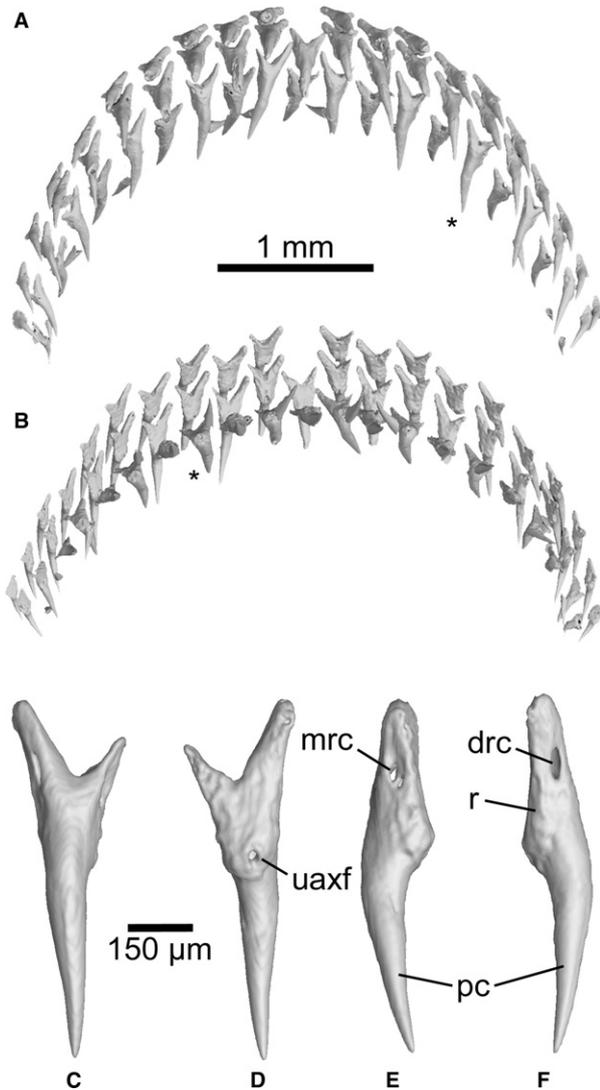

Fig. 9 *Mollisquama* sp., TU 203676, lower jaw and dentition. (A) labial view; (B) lingual view; (C) lateral view. Gap in dentition on Meckel's cartilage due to missing teeth. Asterisks denote teeth shown in Fig. 10.

Fig. 8 *Mollisquama* sp., TU 203676, upper dentition teeth. (A) oral view; (B) viewed from above. (C–F) individual segmentation analysis of an upper tooth (denoted with an asterisk in A,B), in labial, lingual, and lateral views.
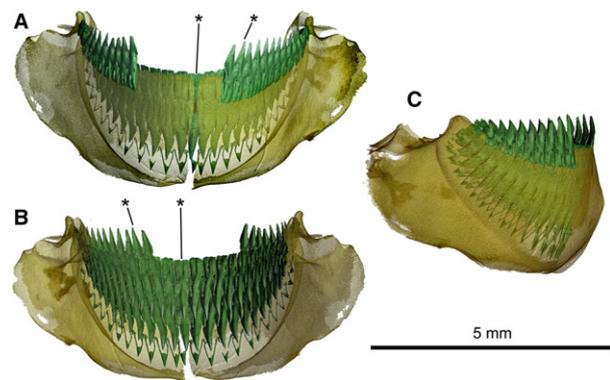
located at the base of the root labial surface. An external foramen connects via a canal to a median internal foramen, located on the lingual bulge of root just below base of the crown. On many of the upper teeth, there are additional small lateral external foramina located on medial and distal root lobes approximately mid-way between their tips and the crown base. The upper tooth crown is needle-like, conical and smooth, without a median labial ridge (cf. *Mollisquama parini*).

The lower teeth are blade-like, and strongly compressed labio-lingually. The crown is medially convex on both labial and lingual surfaces. The labial surface of each tooth crown has an elongate but weakly defined apron, extending basally as far as the lower axial foramen at upper end of labial groove. The lingual surface of the crown exhibits strong median convexity, but there is no uvula, lingual bulge or infundibulum. The root labial surface exhibits a labial hollow that extends about halfway up the root, ending at the lower axial foramen, without a basal notch (cf. *Dalatias*; Adnet & Cappetta, 2001: Fig. 1C). The root lingual surface can have a very weak lingual hollow that does not reach the upper axial foramen (Fig. 10C), or the hollow can be absent (e.g. in the symphyseal tooth; Fig. 10H).

The lower jaw lateral teeth (Fig. 10A–E) have an asymmetrical principal cusp, with the mesial cutting edge slightly angled posteriorly, an upright distal cutting edge, a single distal heel and notch, and a lingual overlapping surface distally below the heel. The labial surface of the root has two labial foramina (mesial and distal) below the apron, and the lingual surface exhibits a single large lingual foramen mesial to the upper axial foramen. Symphyseal teeth (Fig. 10F–I) have a symmetrical principal cusp, paired distal heels separated from the principal cusp by a deep notch, and lingual overlapping surfaces on both sides of the crown. Several labial foramina are present (most of which are small), but only a single lingual foramen is present, to one side of the upper axial foramen.
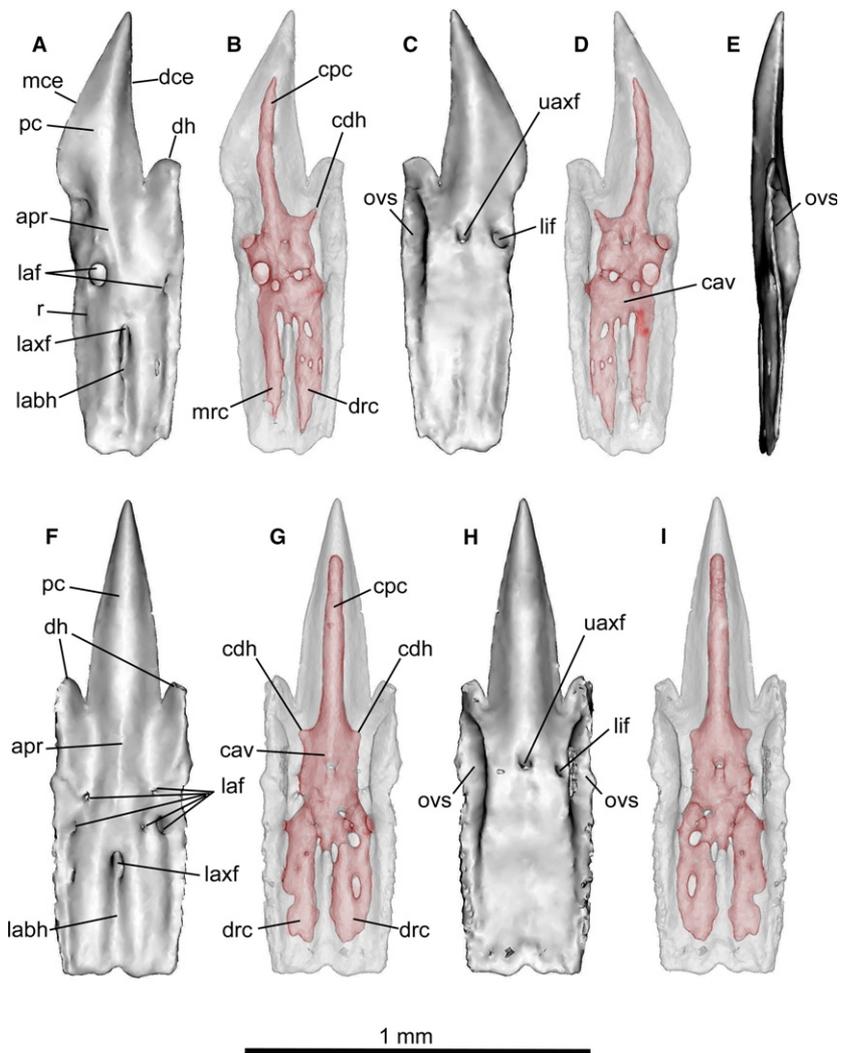
Fig. 10 *Mollisquama* sp., TU 203676. Individual segmentation analyses of lower teeth. (A–E) tooth from lower left row 4; (F–I) symphyseal tooth. Both teeth are from the first unerupted replacement tooth row and are still attached to the jaw (teeth from the functional row in these positions were missing prior to scanning). (A,B,F,G) labial views; (C,D,G,H) lingual views; (E) mesial view of lateral tooth. Teeth are shown as transparent objects to reveal pulp cavity in (B, D,G,I).

1 mm

The lower teeth have a moderately inflated central pulp cavity within the upper part of root (Fig. 10B,D,I). An elongated vertical canal extends apically from the pulp cavity and enters the principal cusp, and a shorter canal extends towards the distal heel but does not enter it. Symphyseal teeth have a canal for the principal cusp flanked by paired heel canals. The main pulp cavity also divides ventrally on each side of the lower axial foramen, giving rise to distal and mesial branches in lower part of the root. A similar arrangement has been described in *Isistius* (Casier, 1961: Fig. 11), but its upper and lower branches of the pulp cavity form a more complex vascular network than in *Mollisquama* sp.

Hyoid arch

The hyomandibula is approximately twice as long as broad and projects laterally from the otic region of the braincase (Fig. 11). The cranio-hyoid articulation is elongated antero-posteriorly and is located on the posterolateral wall of the otic capsule, just anterior to the exit for the glossopharyngeal nerve (a generalized elasmobranch condition; de Beer, 1937). The cartilage has a slight posterior curve proximo-distally. Its dorsal surface is concave, forming a groove which probably corresponds to the muscular furrow (*sensu* Haller, 1926) in *S. acanthias*. The ceratohyal is longer than the hyomandibula and has a prominent flange-like ventral process, with an anteriorly directed blade-like edge on its mid-ventral margin. The ceratohyal is concave laterally. The basihyal is a short, transverse bar, approximately twice as wide as long, with a rounded anterolateral border and a slightly dished dorsal surface with a distinct anteroposterior ridge along the midline. The posterior border of the basihyal is not notched (cf. *Aculeola*; Shirai, 1991: Pl. 28B). The articular surface for the ceratohyal is located on the ventro-posterolateral border of the basihyal.

Muscles

Cephalic musculature in *Mollisquama* sp. has not been completely analyzed, and only the principal jaw muscles (adductor mandibulae, adductor m. superficialis, suborbitalis,
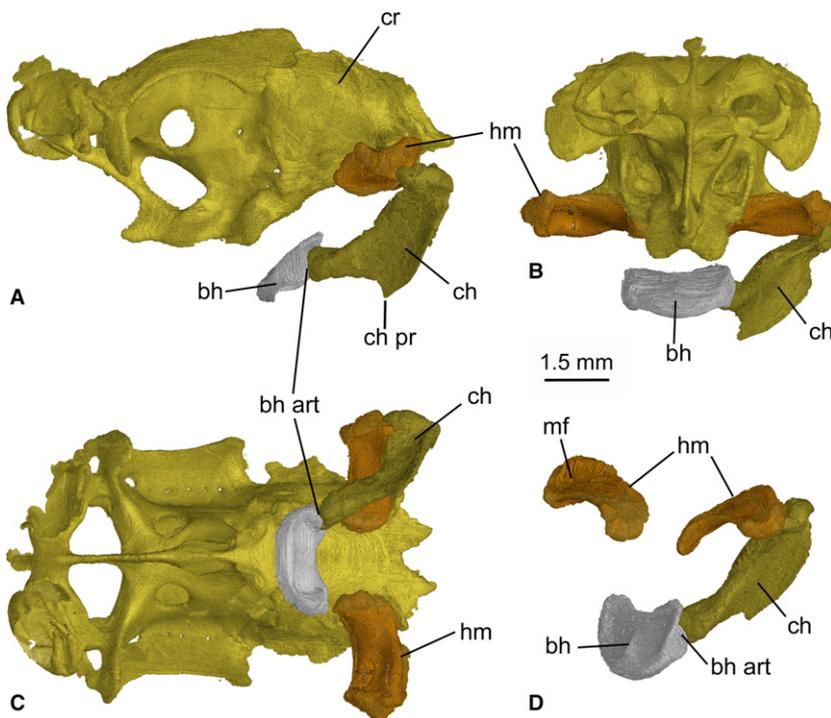
Fig. 11 *Mollisquama* sp., TU 203676, main features of the hyoid arch. (A–C) braincase with hyoid arch attached; (A) left lateral view; (B) anterior view; (C) ventral view; (D) oblique anterolateral view of the hyoid arch. The right ceratohyal is omitted in all views.

constrictor dorsalis) were segmented (Fig. 12). The disc-like adductor mandibulae muscle mass is confined to the posterior half of the jaws, as in other dalatiids, and scan data did not reveal a division between its dorsal and ventral parts. The adductor m. superficialis arises from the ventroposterior part of the adductor mandibulae and inserts on subcutaneous tissue just behind the orbit, as found in many 'squaloids', *Squatina*, and pristiophoroids (Shirai, 1992).

The suborbitalis muscle clearly exceeds the adductor mandibulae in volume, has an extensive origination on the suborbital part of chondrocranium and completely surrounds suborbital carina (see Supporting Information Fig. S4). The left and right suborbitalis muscles meet at a median fascia extending in front of carina and within suborbital fenestra. Suborbitalis muscle mass protrudes anteriorly below the olfactory capsules, contributing to the bulbous cranial profile of *Mollisquama* sp. Just anterior to the adductor mandibulae, the suborbitalis rapidly tapers posterolaterally and inserts onto lateral surface of Meckel's cartilage (either directly or via a tendon; precise condition is uncertain based on scan data).

Phylogenetic analysis and character optimization

Phylogenetic analysis (see Supporting Information Data S1) recovered a monophyletic Dalatiidae, and recovered the euprotomicrinine (*Euprotomicrus*, *Squaliolus*) and dalatiine (*Isistius*, *Dalatias*) groupings of Shirai (1996). *Mollisquama* sp. was recovered as sister to the euprotomicrinine taxa + *Euprotomicroides* (Fig. 13). Parsimony optimization

of character transitions in TnT (Goloboff et al. 2008; Goloboff & Catalano, 2016) identified eight transformations on the stem of Dalatiidae: seven dental characters and one cranial character. Dalatiid sharks exhibited dignathic heterodonty (Ch. 1), vertical or subvertical main cusps on the lower teeth (Ch. 2), higher than broad lower teeth (Ch. 5), bilobed lower tooth apron crenulation (Ch. 20), presence of a labial groove at the basal part of the labial lower tooth face (Ch. 25), presence of an upper tooth axial foramen (Ch. 30), vertical or subvertical primary upper tooth cusps (Ch. 32), and wide separation of nasal capsules (Ch. 43).

Within Dalatiidae, the dalatiine genera exhibited the presence of a 'buttonhole' between the labial and lingual faces of the lower teeth (Ch. 16). The clade including *Mollisquama* + remaining dalatiids exhibited a mesio-lingual foramen equal to or larger than the axial foramen (Ch. 22) and the presence of a median suborbital fenestra (Ch. 52). The euprotomicrinine taxa exhibited an oblique angle to the main cusps of the lower teeth (Ch. 2), loss of the well-developed disto-labial foramen (Ch. 12), and loss of a mesio-lingual foramen (Ch. 21).

The dalatiine taxa exhibited numerous taxon-specific transformations. *Isistius* exhibited loss of an optic pedicel (Ch. 33), presence of separate palatoquadrate elements (Ch. 37), presence of a submandibular accessory cartilage (Ch. 39), and presence of a mandibulo-hyoid ligament (Ch. 40). *Dalatias* exhibited a serrated mesial edge of the lower tooth cusp (Ch. 3), loss of a disto-lingual lower tooth foramen (Ch. 23), presence of a symphyseal plate above the palatoquadrate (Ch. 38), and presence of a subethmoid ridge on the chondrocranium (Ch. 50).
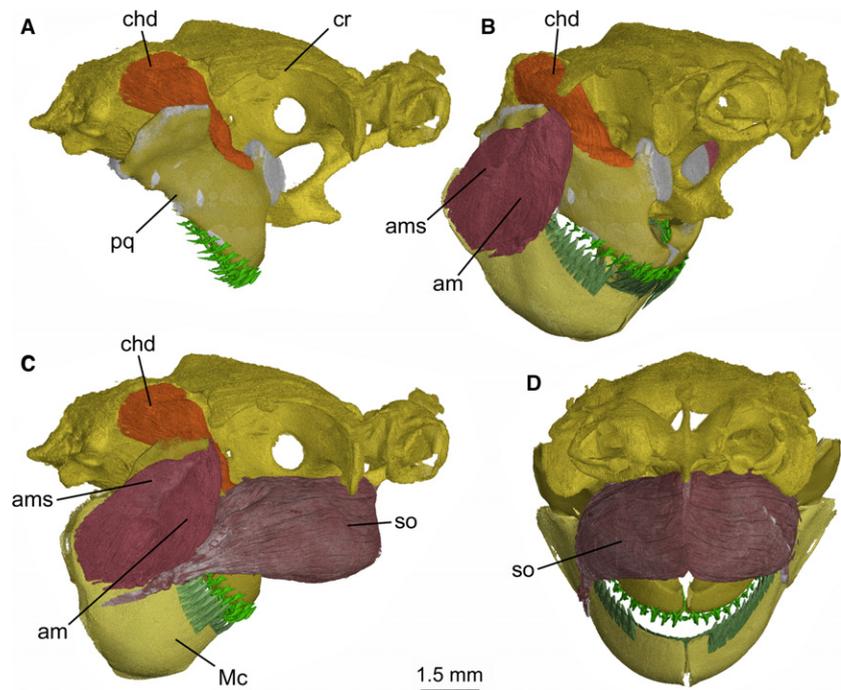
Fig. 12 *Mollisquama* sp., TU 203676, cephalic muscles of the jaws. (A) Right lateral view of the braincase and palatoquadrate, showing the constrictor hyoideus dorsalis extending from below the supraotical shelf into the floor of the orbit; (B) right anterolateral view of the braincase and jaws, showing the extent of the constrictor hyoideus dorsalis, the adductor mandibulae and its superficialis component; (C) right lateral view, showing the suborbitalis and other major jaw muscles; (D) anterior view, showing only the suborbitalis.

Mollisquama sp. exhibited two dental, two chondrocranial, three jaw, and one muscular transformations: absence of a lower tooth mesial heel (Ch. 4) and the basal edge of the lower tooth root medially interrupted by a notch (Ch. 26); absence of an optic pedicel (Ch. 33) and presence of a subethmoid ridge (Ch. 50); upper posterior labial cartilage narrower than anterior (Ch. 41), flat (180°) angle formed by juncture of the upper and lower labial cartilages (Ch. 42), and a pad-like palatoquadrate orbital process (Ch. 47); and shift in location of the origination of the suborbitalis from the interorbital wall to the subethmoid ridge (Ch. 44). At least one dental character transformation was present on each of the internal branches, with the exception of the branch uniting *Euprotomicrus* + *Heteroscymnoides*.

Discussion

Chondrocranium

Chondrocranial morphology of *Mollisquama* sp. resembles that of other dalatiids, but also exhibits several autapomorphic features (Fig. 1). Having the nasal capsules almost united at the midline is a characteristic of the 'Dalatias-group' (Shirai, 1992: char. 18r), which also includes *Dalatias*, *Isistius*, *Oxynotus*, *Euprotomicrus*, and *Squaliolus*. However, given recent molecular data placing *Oxynotus* inside Somniosidae (Straube et al. 2015), this feature may be convergent in this genus. The nasal cartilage of *Mollisquama* sp. (Fig. 2) broadly resembles that illustrated in *Cirrhigaleus barbifer* by Shirai (1992: Pl. 19C), although the cartilage in *Cirrhigaleus* is directed ventrolaterally rather than anteriorly. The nasal cartilages are much larger than

in other taxa included in Shirai (1992)'s 'Dalatias-group', and extend behind the olfactory capsules as far as the inner wall of the olfactory canals. Paired rostral fenestrae occur in most 'squaloid' sharks, *Hexanchus*, *Heptranchias*, and *Pristiophorus*, but are absent in modern galeomophs and batoids. The rostral fenestrae of *Mollisquama* sp. extend behind the nasal capsules and that is also the case for *Hexanchus*, *Zameus*, *Centroscyllium*, *Trigonognathus*, *Dalatias*, *Isistius*, and *Squaliolus*. The rostral fenestrae in *Deania* are located entirely behind the capsules but are confined to the region between them in *Squalus*, *Centrophorus*, and *Cirrhigaleus*. Rostral fenestrae are also present in *Pristiophorus* and hexanchiforms except *Notorynchus* (Holmgren, 1941), but are absent in modern galeomorphs, batoids, and extinct stem elasmobranchs such as hybodonts. *Mollisquama* sp. has a precerebral fontanelle but according to Shirai (1992: char. 13) a fontanelle is absent in *Squaliolus* and *Euprotomicrus*.

Since the ontogeny of *Mollisquama* sp. is unknown, the embryonic derivation of the suborbital carina cannot be verified, but it possibly represents a mid-ventral extension of the embryonic trabecular cartilages. A similar suborbital carina is present in *Squaliolus*, but this form lacks a carinal process and has only a small, incomplete fenestra in its lower border (Shirai, 1992: Pl. 18C). In *Dalatias*, there is only a low carina ('subethmoid ridge'; Shirai, 1992: Pl. 8), which bears a short, anteroventrally directed process that lacks fenestration. Holmgren (1940: Figs 95, 96, 98) described a short basicranial 'keel-process' in 55-mm *Etmopterus* embryos that persists in adults (Holmgren, 1941: Fig. 21). Shirai (1992: char. 48) considered that the process was an etmopterine synapomorphy, but it may be homologous
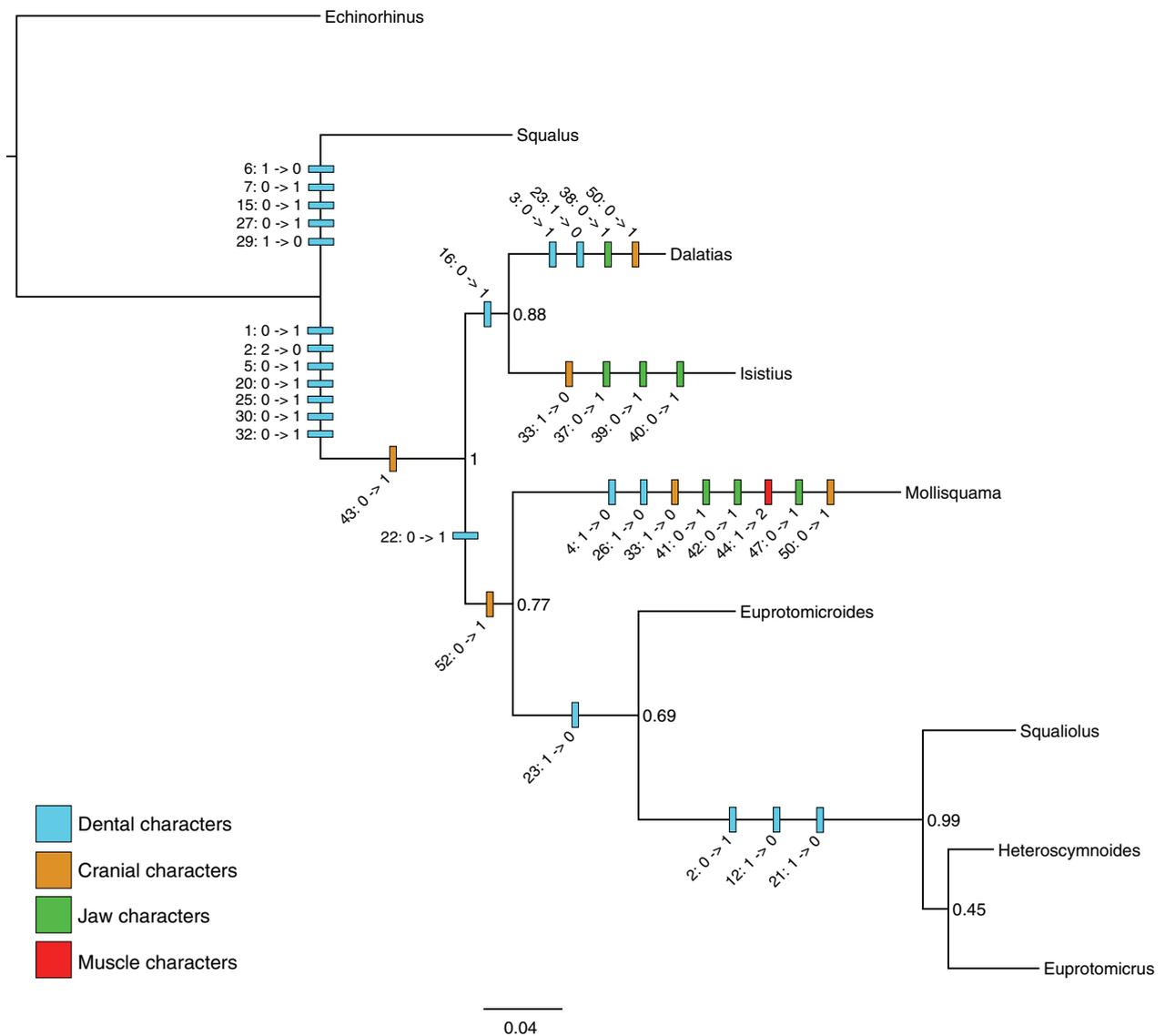
Fig. 13 Combined molecular (ND2) and morphological phylogenetic analysis of dalatiid sharks, with morphological character transformations mapped using parsimony. Tree shown is the maximum clade credibility tree/MAP topology, with clade credibility values. See Data S2, S3 for morphological characters.

with the suborbital carina in *Mollisquama* sp. and *Squaliolus*.

The presence of a basal angle associated with the suborbital carina is restricted systematically, occurring only in certain orbitostylic elasmobranchs (*sensu* Maisey, 1980). Shirai's (1992: 44) claim that the 'presphenoid bolster' of *Chlamydoselachus* and *Squatina* (Holmgren, 1941) "cannot be distinguished from the basal angle of 'squaloid' sharks in form" can be refuted on topological grounds because the bolster is not located at the chordal/prechordal boundary (approximated in adult elasmobranch chondrocrania by the position of the internal carotid foramen; Holmgren, 1941), but lies much farther anteriorly (thus entirely within the inferred domain of the embryonic trabecular cartilage); *Chlamydoselachus* and *Squatina* lack a basal angle at the

chordal/prechordal boundary. Shirai (1992) also claimed that a basal angle is present in pristids (although it was not illustrated). In fact, the pristid basicranium is flat and a basal angle is absent (Holmgren, 1941: 55); no batoid possesses a basal angle of the type described in orbitostylic sharks. Although a suborbital carina occurs in 'squaloids' with a well-developed basal angle, it is sometimes absent. *Centroscyllium* possesses only a rodlike process extending from the ventral midline of the basicranium below the optic foramen (Shirai & Nakaya, 1990: Fig. 2; Shirai, 1992: Pl. 4), and in *Trigonognathus*, the carina is secondarily absent, according to Shirai (1992). The large suborbital space between the basal angle and the nasal capsules in *Trigonognathus* could be considered a fenestra lacking a lower margin, and *Trigonognathus* lacks the suborbitalis muscle (Shirai, 1992:

char. 63), which originates on the carina in *Mollisquama* sp. (see below) and *Squaliolus* (Shirai, 1992: Pl. 38C).

The lateral margin of the supraorbital shelf in *Mollisquama* sp. is slightly curved, rather than deeply indented as in *Squalus* or *Dalatias,* and there is no evidence of a separate profundal foramen. Absence of a profundal canal has been regarded as a derived state uniting *Dalatias* and *Isistius* (Shirai, 1992: char. 104), although one is also absent in *Trigonognathus*. The profundal nerve arrangement is unclear in *Euprotomicrus*, and Shirai (1992) did not identify a profundal foramen in *Squaliolus*. *Mollisquama* sp. lacks the deep embayment of the supraorbital shelf seen in *Dalatias*, anterior to the process. In *Squaliolus* and *Isistius*, the supraorbital shelf is also embayed, but the posterior margin of the process is rounded and merges with the otic region more gradually than in *Dalatias* or *Mollisquama* sp.

The optic pedicel could not be found in *Mollisquama* sp., suggesting that it may be absent, as reported in *Isistius* by Shirai (1992). He also stated that the pedicel fails to reach the eye in *Deania*, *Etmopterus*, *Miroscyllium*, and *Oxynotus,* and that its distal tip forms the origin of three rectus muscles in these taxa. There is clearly some variation in this feature that deserves further analysis and comparison. *Mollisquama* sp. apparently differs from *Euprotomicrus* and *Squaliolus* in lacking an opening for an additional vein from the orbital sinus in the interorbital wall (Shirai, 1992: char. 41).

Shirai (1992: char. 42) regarded the presence of a deep myodome for the external rectus muscle as an apomorphic character within certain dalatiids (e.g. *Euprotomicrus*, *Squaliolus*), and proposed that it arose independently in etmopterids. Although presence of the myodome *sensu* Shirai (1992) may represent a synapomorphy of *Mollisquama* sp., *Euprotomicrus* and *Squaliolus*, the states of this character in dalatiids deserve further scrutiny.

The lateral wall to the trigemino-facialis recess in *Mollisquama* was presumably formed in the embryonic lateral commissure as Holmgren (1940, 1941) found in other modern elasmobranchs. The lateral commissure is sometimes present only as an unchondrified membrane (e.g. *Squalus*), but it is extensively chondrified in *Mollisquama* sp. (Fig. 1C). In *Squalus*, *Etmopterus*, and *Scyliorhinus*, the lateral commissure arises as a dorsal extension of the basal plate and secondarily connects with the otic capsule (de Beer, 1937; Holmgren, 1940; Schaeffer, 1981; Gardiner, 1984). In *Mollisquama* sp., the dorsal end of the commissure merges with the side wall of the braincase below the level of the supraorbital shelf, whereas the commissure in many extinct sharks is confluent with the supraorbital shelf. The commissure is not present in certain batoids and all hexanchids. Contra Shirai (1992), there is no cartilaginous lateral commissure in *Chlamydoselachus* (Allis, 1923; Holmgren, 1941).

The foramen for the hyomandibular branch of the facial nerve in *Mollisquama* sp. is located well posterior to the level of the lateral commissure and to the main trigemino-facial nerve foramen (Fig. 1B,C). A similar arrangement is present in *Oxynotus*, *Isistius*, *Squaliolus*, and *Dalatias*, but in certain other elasmobranchs (e.g. *Chlamydoselachus*, *Notorynchus*, *Squalus*, *Zameus*, *Trigonognathus*), the trigemino-facial and hyomandibular foramina are closer together. The bulbous and rounded basitrabecular processes (*sensu* Shirai, 1992) are not as prominent as in *Zameus* or *Isistius*, however, the basitrabecular process in *Isistius* differs in being confluent with the base of the lateral commissure.

The lateral wall of the otic capsule is flared laterally and forms a prominent and well calcified sphenopterotic ridge (*sensu* Shirai, 1992), as in *Dalatias* and *Squaliolus*; a less extensive ridge is present in *Isistius* and is confined to the anterior part of the otic region. In *Mollisquama* sp., the sphenopterotic and supraorbital shelves are separated by a deep, rounded notch, unlike in other dalatiids. In addition, the posterior end of the supraorbital shelf in *Mollisquama* sp. is downturned below the level of the sphenopterotic ridge, so the two shelves are not confluent as in other elasmobranchs. The sphenopterotic ridge in dalatiids is topographically homologous with the elasmobranch supraotical shelf *sensu* Holmgren (1941) and is probably also homologous with the lateral otic ridge in certain Paleozoic chondrichthyans (e.g. *Orthacanthus*; Schaeffer, 1981). According to Shirai (1992), a sphenopterotic ridge is absent in galeomorphs, but there is a prominent supraotical shelf in *Lamna* (Maisey & Springer, 2013) which, like the sphenopterotic ridge, is located above the origin of the constrictor dorsalis muscle.

The otic region exhibits features that have been implicated in low-frequency semi-directional phonoreception in other elasmobranchs (Maisey & Lane, 2010; and references therein), including absence of a crus between the anterior and posterior semicircular canals. However, no data are available concerning phonoreception in *Mollisquama* sp. or other dalatiids. Posterior to the otic region, the paired endolymphatic foramina and perilymphatic fenestrae are separate as is typical for most elasmobranchs, but they are confluent in *Zameus* and *Isistius* (most parsimoniously resolved as independent specializations in these genera; Shirai, 1992: char. 49).

The pattern of chondrocranial mineralization in *Mollisquama* sp. (Fig. 4) approximates that observed in 25-cm juvenile *Squalus acanthias* (Benzer, 1944), suggesting either that the *Mollisquama* sp. specimen is a juvenile (as evidenced by a healed umbilical scar and claspers that were not firm; Grace et al. 2015) or that calcification was arrested early in its ontogeny. The suborbital carina is, nevertheless, strongly mineralized in *Mollisquama* sp., whereas no calcification is present in the ethmoid region of 25-cm *Squalus*.

Jaws and hyoid arch

The articular process of the palatoquadrate extends ventrocaudally from the arch piece and bears an articular condyle

for the lower jaw, but the process is wider and more trapezoidal in shape than in *Squalus* and instead resembles the process in *Etmopterus*, *Cirrhigaleus*, *Zameus*, and *Dalatias* (Shirai, 1992: Pls. 25C, 26A,B,D); the articular process in *Isistius* is notably smaller than in these other taxa (Shirai, 1992: Pl. 26C). The palatoquadrate posterior margin is gently convex; by contrast, this margin is almost straight in *Zameus* and is slightly concave in *Cirrhigaleus* and *Dalatias* (Shirai, 1992: Pl. 26).

The *Mollisquama* orbital process resembles that of *Squalus* but is considerably lower and wider. In *Mollisquama* sp., the orbital process is the only direct articulation between the mandibular arch and chondrocranium, unlike in *Squalus* where there is a second articulation when the jaws are fully retracted, between the dorsal margin of the palatoquadrate symphysis and the basicranium (Wells, 1917). In *Squalus*, the orbital process is positioned against the medioposterior wall of the orbit when the jaws are in a retracted position, forming a sliding joint between the process and the orbital groove when the jaws are protracted. By comparison, the range of motion between the orbital process and basicranium in *Mollisquama* sp. is undoubtedly limited both by the shortness of the orbital process and by the massive suborbitalis muscle. Additionally, the deep embayment in the anterior part of the palatoquadrate in *Mollisquama* sp. separates the jaws from the basicranium, probably precludes direct articulation between them when the jaws are fully retracted. Shirai (1992) noted the presence of a separate cartilaginous median symphyseal plate in *Dalatias*; this is absent in *Mollisquama* sp. as well as in other dalatiids investigated by Shirai (1992).

The palatoquadrate main bar in *Mollisquama* sp. has a gently rounded, convex outer surface which merges imperceptibly with the muscular process and adductor attachment surface, as in *S. acanthias* (Wolfram, 1984) and many other elasmobranchs. By contrast, in *Dalatias*, *Isistius*, *Squaliolus*, and *Euprotomicrus*, a deep, oblique sulcus is present between the adductor attachment area and the tooth-bearing region of the palatoquadrate main bar (see Supporting Information Fig. S5A). Cartilage within this sulcus is sometimes difficult to resolve by segmentation analysis of tomographic scans, suggesting that it is weakly mineralized.

The quadrate concavity in *Squalus* is formed entirely in fibrous connective tissue instead of on the palatoquadrate cartilage itself (Wolfram, 1984), whereas the concavity in *Mollisquama* is located on the cartilage. According to Hotton (1952: 494), modern sharks with a quadrate concavity on the palatoquadrate generally have a slender, non-suspensory hyomandibula, whereas those without this concavity have a short, stout, suspensory hyomandibula. *Mollisquama* is thus an exception to this generalization because its hyomandibula is short and suspensory, yet a quadrate concavity is present on the palatoquadrate.

In *Mollisquama* sp., *Dalatias*, *Euprotomicrus*, and *Squaliolus*, the articular cotylus of the mandibular joint is located

on a short outer process that extends laterally from the posterior extremity of Meckel's cartilage, as Haller (1926) described in *S. acanthias* and the cotylus is offset posteroventrally with respect to the occlusal surface of the lower dentition. The widespread systematic occurrence of this arrangement suggests that it may be primitive for dalatiids generally. By contrast, there is no outer process in *Isistius* and its articular cotylus is located immediately behind the posteriormost teeth with no ventral offset from the occlusal surface (see Fig. S5B).

The Meckelian symphysis in many 'squaloid' elasmobranchs extends for only a short distance below the tooth-bearing region (e.g. *Squalus*, *Euprotomicrus*, *Squaliolus*). By contrast, the symphysial region is relatively deep in *Mollisquama* sp., *Dalatias*, and *Isistius*. A gap below the symphysis, like that in *Mollisquama* sp. (Fig. 6H,I), is also found in *Dalatias*, *Isistius*, and *Squaliolus*, but differs in extent and shape. In *Dalatias*, the symphyseal gap occupies approximately half the symphysial region as in *Mollisquama* sp. but is not parallel-sided; instead, it widens and then narrows again farther ventrally, imparting a lenticulate shape. In *Isistius*, the gap occupies only the lower 30% of the symphysial region, forming a triangular notch. In *Squaliolus*, the gap is shaped as in *Dalatias* but the symphysis above the gap is shorter.

Mollisquama sp. lacks flap-like accessory cartilages behind the lower jaw, as found in *Isistius* (Shirai, 1992: char. 59). It also lacks a process for the mandibulo-hyoid ligament like that of *Isistius* (Shirai, 1992: char. 61) and seems to lack a small median 'ventral drop' cartilage like that identified by Shirai (1992: char. 60) in *Centroscymnus*, *Scymnodon*, and *Zameus*.

In *S. acanthias*, the lower and upper posterior labials are contained in a fold of skin forming the corner of the mouth, and the upper anterior labial underlies a more anterior separate fold in the skin. In *Mollisquama* sp., by contrast, there are no upper labial furrows or lower labial folds (Dolganov, 1984; Grace et al. 2015). The labials in *Mollisquama* sp. thus resemble a dental mouth prop by keeping the oral margin clear of the dentition.

In the hyoid arch of *Mollisquama* sp. (Fig. 11), the hyomandibula-ceratohyal joint is located farther behind the mandibular knob than in most elasmobranchs, a potential synapomorphy with *Isistius* and *Dalatias* (Shirai, 1992). The basihyal-ceratohyal joint is located along the posterolateral margin of the basihyal (a systematically widespread condition), not on the basihyal posteroventral surface as described in *Isistius* by Shirai (1992).

Teeth and dentition

Grace et al. (2015) gave the following tooth formulae for TU 203676: upper jaw 9-1-9, lower jaw 15-1-15; based on scan data, the upper jaw tooth formula is here revised to 10-1-10 but the lower is correct. In the holotype of *M.*

parini, Dolganov (1984) provided the following tooth formula; upper 12-1-12, lower 15-1-15.

According to Dolganov (1984), a longitudinal ridge is present at the midline of the labial surface in the holotype of *M. parini*, a feature he used to distinguish the taxon from *Dalatias*. However, a comparable ridge is absent on upper teeth in *Mollisquama* sp. A median labial ridge is present on some (but not all) the upper teeth in modern *Scymnodalatias albicauda* illustrated by Herman et al. (1989: pl. 17). A median ridge is also present in Eocene upper teeth referred to *Scymnodalatias cigalafulgosii* (Cappetta, 2012: fig. 113A, B, D). As far as can be determined, this ridge does not occur in other dalatiid upper teeth. Dolganov (1984) commented that vascularization of the upper teeth in *M. parini* is the same as in *Scymnodalatias* and *Euprotomicroides zantedeschia*, and that *M. parini* upper tooth morphology is more similar to *Euprotomicroides* than to *Scymnodalatias.*

Lower jaw teeth in the *Mollisquama* sp. specimen (Fig. 10) closely resemble those described by Cigala Fulgosi (1996: fig. 4) from the holotype of *M. parini*. As in *Euprotomicroides*, the lower tooth roots in *Mollisquama* sp. lack a 'button-hole' ('boutonnière') enclosing the lower axial foramen like modern *Dalatias* and *Isistius* (Casier, 1961). Tooth roots are taller in the new specimen of *Mollisquama* sp. than in other dalatiids, although comparable elongation of the root occurs in *Scymnodalatias*. The original length of the roots is uncertain in the holotype of *M. parini* because their basal parts are no longer present, possibly from damage by formalin (Cigala Fulgosi, 1996). According to Dolganov (1984), the roots of all the lower teeth in the holotype of *M. parini* have a deep basal sulcus, but this is absent or only weakly present in the teeth of the second specimen.

In some dalatiids, the upper and lower tooth arcades of the dentition are not aligned with each other laterally or posteriorly, resulting in a distinct underbite (i.e. the lower teeth are lateral to the uppers; e.g. *Mollisquama*, *Squaliolus*, *Euprotomicrus*, *Isistius*; see Supporting Information Fig. S6), although this is only weakly developed in *Mollisquama*. In *Isistius*, there is no occlusion at all between upper and lower teeth, resulting in an underbite that extends around the entire jaw (Shirai & Nakaya, 1992). Although an underbite is an unusual feature of elasmobranchs that may represent a functional adaptation related to feeding, it is also a potentially apomorphic feature within certain elasmobranchs.

Muscles

The suborbitalis muscle is large in many dalatiids (Luther, 1908; Shirai, 1992), but it seldom approaches the size found in *Mollisquama* sp. Following Shirai (1992), we regard the union of the left and right suborbitalis muscles at the ventral midline as a derived feature, uniting *Mollisquama* sp. with at least some dalatiids, although further investigation is required to determine the systematic distribution of this arrangement in the group. The posterior parts of the suborbitalis muscles also meet at the ventral midline of the basicranium in pristiophorids (Luther, 1908: Pl. 2-17; Shirai, 1992: Pl. 40C), but a fascia between them is absent and there is no suborbital carina. Shirai (1992) characterized the origin of the suborbitalis in dalatiids as being located on the interorbital wall. In *Mollisquama* sp., however, the muscle clearly originates on the suborbital carina below the orbit. Moreover, the muscle also seems to originate below the orbit in *Dalatias* and *Squaliolus* (Shirai, 1992: Pl. 38A,C) and may represent a synapomorphy of these taxa.

Phylogenetic analysis and dalatiid cranial evolution

The placement of *Mollisquama* sp. in the present analysis, based on a 50% majority-rule consensus topology derived from Bayesian analysis of combined ND2 and morphology data (Fig. 13), differs from the placement of the taxon in the likelihood-based ND2-only phylogeny of Grace et al. (2015), in which *Mollisquama* sp. was recovered as sister to *Dalatias* + *Isistius*, although the Grace et al. relationships among the taxa in common to both analyses was recovered in the posterior distribution of trees. Placement of *Mollisquama* sp. as sister to a group comprising *Euprotomicroides*, *Squaliolus*, *Heteroscymnoides* and *Euprotomicrus* broadly resembles the tree presented in Claes & Mallefet (2009, Fig. 3), which was based on dental characters from Adnet & Cappetta (2001), and which recovered a clade comprised of *Mollisquama* + *Euprotomicroides*, separate from the dalatiine taxa. However, the data supporting the clade in this figure is unclear, as Adnet & Cappetta (2001) did not include *Mollisquama* in their matrix of dental characters due to the lack of dental information in the original species description (Adnet & Cappetta, 2001, p. 237). By coding dental information for *Mollisquama,* our analysis provides the first complete dental dataset for dalatiid sharks.

The results of the present analysis indicate that *Mollisquama* sp. exhibits a wider degree of character transformation across more of the included anatomical systems than the other dalatiids (Fig. 13), thus expanding the morphospace disparity of the family and indicating a potentially unique morphospace region for *Mollisquama* sp. that is somewhat corroborated by its phylogenetic placement between the dalatiine and euprotomicrinine taxa. However, due to the presence of missing data for *Euprotomicroides* and *Heteroscymnoides*, the low support values, the low molecular marker coverage [1 open reading frame (ORF)] and type (mitochondrial DNA), and the taxonomic scale of the analysis, we must contextualize such results in cautious terms. Because taxonomic breadth can affect both the selection and conceptualization of anatomical characters and their states, and the resulting inferred synapomorphies (Scotland et al. 2003), we have favored the term 'transformations' over apomorphy-based definitions in discussing such character patterns in dalatiids.

The functional significance of these transformations in *Mollisquama* sp. remains unclear. Under the hypothesis that *Mollisquama* sp. exhibits an ectoparasitic feeding strategy, the configuration of the labial cartilages may be potentially advantageous for orienting the biting surface during approach toward and attachment to prey animals, and the pad-like orbital process may be important both as antero-posterior structural support against forward-momentum impact of the shark following acceleration toward prey animals (Jones, 1971; Shirai & Nakaya, 1992). Similarly, the origination, contour, and reinforced structure of the suborbitalis muscle may increase bite-force strength and could be related to trophic specialization by *Mollisquama* sp. on a difficult prey tissue, such as blubber, an idea potentially supported by the capture of *Mollisquama* sp. during a cetacean survey (Grace et al. 2015). Alternatively, given the small size of *Mollisquama* sp., these structures may simply be a scaling artifact necessary for a small oral surface to generate the forces required for ectoparasitism. Many dalatiid prey species are considered active apex predators (white sharks, Gallo-Reynoso et al. 2005; Hoyos-Padilla et al. 2013; killer whales, Dwyer & Visser, 2011), and the unique *Mollisquama* sp. specializations may enable such a small predator to balance the successful removal of a tissue plug against increased physical risk of damage through increased bite efficiency. However, unlike the known dalatiid ectoparasite *Isistius*, which possesses both an apomorphic 'collar' and unusual bioluminescence spectrum thought to play roles in ectoparasitic predation (Claes & Mallefet, 2009), little is known about *Mollisquama* sp. ventral bioluminescence. Additionally, description of the *Mollisquama* sp. oropharynx, and potential muscular specializations for negative pressure generation (as in the *Isistius* predation mechanism; Shirai & Nakaya, 1992), remains outstanding. The suggestion of an ectoparasitic feeding strategy in *Mollisquama* sp. is therefore provisional.

Conclusions

The success of the *Mollisquama* sp. imaging provides a unique and expanded opportunity to assess internal anatomy from an extremely rare and diminutive midwater specimen. The *Mollisquama* sp. chondrocranium, jaws, and primary musculature suggest specializations typical of dalatiid ectoparasitism (Figs 1–12). Like other dalatiids, *Mollisquama* sp. exhibits dignathic heterodonty (Figs 7–10), conforming to the 'cutting-clutching' pattern *sensu* Cappetta (2012). *Mollisquama* sp. appears to be uniquely diagnosable based on the presence of an elaborated carinal process (Fig. 1), the shape of the palatoquadrate orbital process (Fig. 6), the unusual planar configuration of the labial cartilages and the apparent absence of labial folds (Fig. 7), and the location of origination, and contour, of the suborbitalis muscle (Fig. 12). Additionally, the absence of an upper-tooth ridge (Fig. 8) and tooth

counts, along with features identified by Grace et al. (2015), distinguish *Mollisquama* sp. from *M. parini* Dolganov (1984). Multiple character transformations in the context of dalatiid phylogeny suggest *Mollisquama* sp. contributes significantly to dalatiid morphological disparity, and the taxon appears to be somewhat intermediate between the dalatiine and euprotomicrinine types, although the functional significance of these transformations remains unclear. The successful recovery of soft tissue information from the *Mollisquama* scan underscores an advantage of synchrotron-based microtomography over existing soft tissue microCT visualization techniques such as phosphotungstic acid (PTA; Metscher, 2009) or diceCT (Gignac et al. 2016). Synchrotron approaches do not require treatment of specimens with contrast-enhancing chemicals and may thus be preferred for visualizing soft tissue data in cases where the number of available specimens is extremely limited.

Author contributions

G.N. and M.G. conceived the study. J.S.S.D. transported the specimen, processed the scan data, and generated the 3-D reconstructions. J.G.M. wrote the anatomical description. A.P. transported the specimen, served as ESRF liason, and edited the manuscript. M.D. and H.B. provided specimen paperwork and input on the manuscript. All authors approved the final version.

References

Adnet S, Cappetta H (2001) A palaeontological and phylogenetical analysis of squaliform sharks (Chondrichthyes: Squaliformes) based on dental characters. *Lethaia* **34**, 234–248.

Allis EP (1923) The cranial anatomy of *Chlamydoselachus anguineus*. *Acta Zool* **4**, 123–221.

de Beer GR (1937) *The Development of the Vertebrate Skull*. Oxford: Oxford University Press.

Benzer P (1944) Morphology of calcification in *Squalus acanthias*. *Copeia* **1944**, 217–224.

Best PB, Photopoulou T (2016) Identifying the 'demon whale-biter': patterns of scarring on large whales attributed to a cookie-cutter shark *Isistius* sp. *PLoS One* **11**, e1052643.

Cappetta H (2012) Chondrichthyes. Mesozoic and Cenozoic Elasmobranchii: teeth. In: *Handbook of Palaeoichthyology*. (ed. Schultze H-P), pp. 1–512, Munich: Verlag Dr. Friedrich Pfeil.

de Carvalho MR (1996) Higher-level elasmobranch phylogeny, basal squaleans, and paraphyly. In: *Interrelationships of Fishes*. (eds Stiassny MLJ, Parenti LR, Johnson GD), pp. 35–62. New York: Academic Press.

Casier E (1961) Transformations des systèmes de fixation et de vascularisation dentaires dans l'évolution des sélaciens du sous-ordre des squaliformes. *Mém Mus R His Nat Belg* **65**, 1–55.

Cigala Fulgosi F (1996) Rare oceanic deep water squaloid sharks from the Lower Pliocene of the Northern Apennines (Parma Province, Italy). *B Soc Paleontol Ital* **34**, 301–322.

Claes J, Mallefet J (2009) Bioluminescence of sharks: first synthesis. In: *Bioluminescence in Focus – A Collection of Illuminating Essays*. (ed. Victor Benno Meyer-Rochow), pp. 51–65, Kerala: Research Signpost.

Dolganov VN (1984) A new shark from the family Squalidae caught on the Naska Submarine Ridge. *Zool Zh* **63**, 1589–1591.

Dwyer SL, Visser IN (2011) Cookie cutter shark (*Isistius* sp.) bites on cetaceans, with particular reference to killer whales (Orca) (*Orcinus orca*). *Aquat Mamm* **37**, 111–138.

El-Toubi MR (1949) The development of the chondrocranium of the spiny dogfish, *Acanthias vulgaris* (*Squalus acanthias*). Part I. Neurocranium, mandibular and hyoid arches. *J Morphol* **84**, 227–279.

Gallo-Reynoso JP, Le Boeuf BJ, Figueroa AL, et al. (2005) Los pinnípedos de Isla Guadalupe. In: *Isla Guadalupe: Hacia su Restauración y Conservación*. (eds Santos-del-Prado K, Peters E), pp. 171–201. Ciudad de México: Instituto Nacional de Ecología.

Gardiner BG (1984) The relationships of the palaeoniscid fishes, a review based on new specimens of *Mimia* and *Moythomasia* from the Upper Devonian of Western Australia. *Bull Br Mus Nat Hist Geol* **37**, 173–428.

Gignac PM, Kley NJ, Clarke JA, et al. (2016) Diffusible iodine-based contrast-enhanced computed tomography (diceCT): an emerging tool for rapid, high-resolution, 3-D imaging of metazoan soft tissues. *J Anat* **228**, 889–909.

Goloboff PA, Catalano SA (2016) TNT version 1.5, including a full implementation of phylogenetic morphometrics. *Cladistics*, **32**, 221–238.

Goloboff PA, Farris JS, Nixon KC (2008) TNT, a free program for phylogenetic analysis. *Cladistics*, **24**, 774–786.

Grace MA, Doosey MH, Bart HL, et al. (2015) First record of *Mollisquama* sp. (Chondrichthyes: Squaliformes: Dalatiidae) from the Gulf of Mexico, with a morphological comparison to the holotype description of *Mollisquama parini* Dolganov. *Zootaxa* **3948**, 587–600.

Haller G (1926) Ueber die Entwicklung, den Bau und die Mechanik des Kieferapparates des Dornhais (*Acanthias vulgaris*). *Z Mikrosk Anat Forsc* **5**, 749–793.

Hayashi T, Higo E, Orito H, et al. (2015) Postmortem wounds caused by cookie-cutter sharks (*Isistius* species): an autopsy case of a drowning victim. *Forensic Sci Med Pat* **11**, 119–121.

Herman J, Hovestadt-Euler M, Hovestadt DC (1989) Contributions to the study of the comparative morphology of teeth and other relevant ichthyodorulites in living supraspecific taxa of chondrichthyan fishes. Part A: Selachii. No. 3: Order: Squaliformes Families: Echinorhinidae, Oxynotidae and Squalidae. *Bull Inst R Sci Nat Belg Biol*, **59**, 101–157.

Holmgren N (1940) Studies on the head in fishes. Part I. Development of the skull in sharks and rays. *Acta Zool* **21**, 51–267.

Holmgren N (1941) Studies on the head in fishes. Part II. Comparative anatomy of the adult selachian skull with remarks on the dorsal fins in sharks. *Acta Zool* **22**, 1–100.

Hotton N III (1952) Jaws and teeth of American xenacanth sharks. *J Paleontol*, **48**, 9–500.

Hoyos-Padilla M, Papastamatiou YP, O'Sullivan J, et al. (2013) Observation of an attack by a cookiecutter shark (*Isistius brasiliensis*) on a White Shark (*Carcharodon carcharias*). *Pac Sci* **67**, 129–134.

Jollie M (1971) Some developmental aspects of the head skeleton of the 35–37 mm *Squalus acanthias* foetus. *J Morphol* **133**, 17–40.

Jones EC (1971) *Isistius brasiliensis*, a squaloid shark, probable cause of crater wounds on fishes and cetaceans. *Fish Bull Natl Oc At* **69**, 791–798.

Luther A (1908) Untersuchungen über die vom N. trigeminus innervierte Muskulatur der Selachier (Haie und Rochen). *Acta Soc Sci Fenn* **36**, 1–168.

Maisey JG (1980) An evaluation of jaw suspension in sharks. *Am Mus Novit* **2706**, 1–17.

Maisey JG, Lane JA (2010) Labyrinth morphology and the evolution of low frequency phonoreception in elasmobranchs. *C R Palevol* **9**, 289–309.

Maisey JG, Springer VG (2013) Chondrocranial morphology of the Salmon Shark, *Lamna ditropis*, and the Porbeagle, *L. nasus* (Lamnidae). *Copeia* **2013**, 378–389.

Makino Y, Tachihara K, Ageda S, et al. (2004) Peculiar circular and C-shaped injuries on a body from the sea. *Am J Forensic Med Pathol* **25**, 169–171.

Metscher B (2009) MicroCT for comparative morphology: simple staining methods allow high-contrast 3D imaging of diverse non-mineralized animal tissues. *BMC Physiol* **9**, 11.

Munk O, Jørgensen JM (1988) Putatively luminous tissue in the abdominal pouch of a male dalatiine shark, *Euprotomicroides zantedeschia* Hulley & Penrith, 1966. *Acta Zool* **69**, 247–251.

Paganin D, Mayo S, Gureyev TE, et al. (2002) Simultaneous phase and amplitude extraction from a single defocused image of a homogeneous object. *J Microsc* **206**, 33–40.

Papastamatiou YP, Wetherbee BM, O'Sullivan J, et al. (2010) Foraging ecology of cookiecutter sharks (*Isistius brasiliensis*) on pelagic fishes in Hawaii, inferred from prey bite wounds. *Environ Biol Fishes* **88**, 361–368.

Ribéreau-Gayon A, Rando C, Schuliar Y, et al. (2017) Extensive unusual lesions on a large number of immersed human victims found to be from cookiecutter sharks (*Isistius* spp.): an examination of the Yemenia plane crash. *Int J Legal Med* **131**, 423–432.

Schaeffer B (1981) The xenacanth shark neurocranium, with comments on elasmobranch monophyly. *Bull Am Mus Nat Hist* **169**, 1–66.

Scotland RW, Olmstead RG, Bennett JR (2003) Phylogeny reconstruction: the role of morphology. *Syst Biol* **52**, 539–548.

Shirai S (1992) *Squalean Phylogeny: A New Framework of 'Squaloid' Sharks and Related Taxa*. Sapporo: Hokkaido University Press.

Shirai S (1996) Phylogenetic interrelationships of neoselachians (Chondrichthyes: Euselachii). In: *Interrelationships of Fishes*. (eds Stiassny MLJ, Parenti LR, Johnson GD), pp. 9–34. New York: Academic Press.

Shirai S, Nakaya K (1990) A new squalid species of the genus *Centroscyllium* from the emperor seamount chain. *Jpn J Ichthyol* **36**, 391–398.

Shirai S, Nakaya K (1992) Functional morphology of feeding apparatus of the cookie-cutter shark, *Isistius brasiliensis* (Elasmobranchii, Dalatiinae). *Zool Sci* **9**, 811–821.

Stehmann M, Kukuev E, Konovalenko I (1999) Three new adult records of the oceanic longnose pygmy shark, *Heteroscymnoides marleyi*, from the southeastern Atlantic and southeastern Pacific (Chondrichthyes, Squaliformes, Squalidae). *J Ichthyol* **39**, 606–615.

Straube N, Li C, Claes JM, et al. (2015) Molecular phylogeny of Squaliformes and first occurrence of bioluminescence in sharks. *BMC Evol Biol* **15**, 162.

Wells GA (1917) The skull of *Acanthias vulgaris*. *J Morphol* **28**, 417–443.

Wolfram KE (1984) *The Functional Anatomy of the Jaw Suspension of Notorynchus Cepedianus* (Chondrichthyes, Selachii), with Application to Fossil Forms. Lincoln: University of Nebraska.

Supporting Information

Additional Supporting Information may be found in the online version of this article:

Fig. S1. *Mollisquama* sp., TU 203676; (A,B) anterodorsal segmentation views of the braincase (gold), indicating the prefrontal fontanelle (A) and membranous dura (pale blue in B); (C) sagittal slice through head showing dura.

Fig. S2. *Mollisquama* sp., TU 203676, transverse section through primary postorbital process and lateral commissure.

Fig. S3. *Mollisquama* sp., TU 203676, braincase rendered as a semi-transparent object in dorsal view, anterior to left, showing the location of paired endolymphatic foramina and perilymphatic fenestrae relative to other landmark features.

Fig. S4. *Mollisquama* sp., TU 203676, sagittal section with suborbitalis muscle rendered in false-color (red) to illustrate the encirclement of the suborbital carina by the muscle.

Fig. S5. Illustrations of novel characters and states in the dalatiid morphological data.

Fig. S6. Underbite disparity in dalatiids.

Data S1. Supplementary methods.

Data S2. Character list.

Data S3. Matrix of dalatiid morphological characters.